Published in final edited form as:
*Proteins*. 2010 April ; 78(5): 1153–1162. doi:10.1002/prot.22635.

# The effect of calcium on the conformation of cobalamin transporter BtuB

**Binquan Luan**[*,†], **Rogan Carr**[*], **Martin Caffrey**[‡], and **Aleksei Aksimentiev**[*,§,1]

[*] Department of Physics, University of Illinois, Urbana, IL [†] Physical Science Division, IBM T. J. Watson Research Center, Yorktown Heights, NY [‡] Membrane Structural and Functional Biology Group, University of Limerick, Limerick, Ireland [§] Beckman Institute for Advanced Science and Technology, University of Illinois, Urbana, IL

## Abstract

BtuB is a $\beta$-barrel membrane protein that facilitates transport of cobalamin (vitamin $B_{12}$) from the extracellular medium across the outer membrane of *Escherichia coli*. It is thought that binding of $B_{12}$ to BtuB alters the conformation of its periplasm-exposed N-terminal residues (the TonB box), which enables subsequent binding of a TonB protein and leads to eventual uptake of $B_{12}$ into the cytoplasm. Structural studies determined the location of the $B_{12}$ binding site at the top of the BtuB's $\beta$-barrel, surrounded by extracellular loops. The structure of the loops, however, was found to depend on the method used to obtain the protein crystals, which—among other factors—differed in calcium concentration. Experimentally, calcium concentration was found to modulate the binding of the $B_{12}$ substrate to BtuB. In this study, we investigate the effect of calcium ions on the conformation of the extracellular loops of BtuB and their possible role in $B_{12}$ binding. Using all-atom molecular dynamics, we simulate conformational fluctuations of several X-ray structures of BtuB in the presence and absence of calcium ions. These simulations demonstrate that calcium ions can stabilize the conformation of loops 3–4, 5–6 and 15–16 and thereby prevent occlusion of the binding site. Furthermore, binding of calcium ions to extracellular loops of BtuB was found to enhance correlated motions in the BtuB structure, which is expected to promote signal transduction. Finally, we characterize conformation dynamics of the TonB box in different X-ray structures and find an interesting correlation between the stability of the TonB box structure and calcium binding.

## Introduction

Being unable to synthetize all cofactors required for their metabolism, gram-negative bacteria have developed an elaborate mechanism to import scarce nutrients from the environment. The import mechanisms for many micronutrients such as cobalamins (vitamin $B_{12}$) and iron siderophores are thought to share the following common principle (1,2). An outer membrane protein (OMP) binds the target nutrient from the extracellular environment with a very high (nM) affinity, which is required to effectively scavenge nutrients of low concentration. Release of the nutrients by the OMP to the periplasm requires an energy input, which is delivered by a special periplasmic protein—TonB in the case of both cobalamin and iron siderophore transport. A protein complex associated with the inner membrane uses the proton-motive force to energize TonB (1). In its energized form, TonB binds to a conserved sequence of the OMP's periplasm-exposed residues (the TonB box) facilitating—by a yet unknown mechanism—the

[1]corresponding author. Address: 1110 W. Green St., Department of Physics, University of Illinois, Urbana, IL 61801, U.S.A., Tel.: (217) 333-6495, aksiment@uiuc.edu.

release of the bound nutrient to the periplasm. In this manuscript we focus on the OMP BtuB and investigate the structural changes it undergoes when performing the import of cobalamins into bacteria's periplasm.

Several X-ray structures of BtuB have been determined to date (3–5). The first set of structures (3) revealed a 22-strand $\beta$-barrel linked by 11 extracellular loops and 10 periplasmic turns and a hatch domain located inside the barrel, Fig. 1a. One of the structures (Protein Data Bank (PDB) ID: 1NQH) revealed a $B_{12}$ binding site located on top of the hatch domain and surrounded by the extracellular loops. Another two structures from the same study (PDB IDs: 1NQG and 1NQE) demonstrated that the presence of calcium ions facilitates the ordering of loops. Remarkably, the conformation of the first three residues ($Asp^6$, $Thr^7$ and $Leu^8$) in the TonB box were observed to be correlated with binding ligand ($B_{12}$), which led to the proposal that this set of structures provide direct evidence for the allosteric interactions between cobalamin binding and the conformation of the TonB box (3). This proposal is at variance with the electron paramagnetic resonance (EPR) data (6), which suggested substrate-induced unfolding of the N-terminal part of the protein that includes the TonB box. The most recent structure (4) captured BtuB in complex with TonB, providing direct structural information about the mechanism of TonB interaction with the TonB box. That structure suggested the possibility of a mechanical removal of the hatch domain from the barrel, a scenario that was recently investigated by MD simulations (7). To crystallize BtuB, both structural studies (3, 4) relied on the sitting-drop vapor diffusion crystallization method (8), which we refer to hereafter as the *in surfo* method (9).

Yet another structure of BtuB (5) was obtained using the lipidic cubic mesophase crystallization method (10,11), referred hereafter as the *in meso* method. Compared to *in surfo*-grown BtuB crystals, crystals obtained using the *in meso* technique (10) contain fewer or no metal ions (5,12). The *in meso* and *in surfo* crystallization methods are known to produce different crystal packing of the same protein, which recently permitted reconstruction of a protein structure with a minimum of crystallization artifacts (13). The overall architecture of the *in meso* structure of BtuB (PDB ID: 2GUF) is similar to that of the *in surfo* structure, however considerable structural differences are evident in the organization of the extracellular loops and the conformation of the TonB box (5). Specifically, the loop 15–16 of the *in meso* structure is placed directly above the hatch domain, whereas the same loop of the *in surfo* structure is positioned at the edge of the barrel, Fig. 1b. The TonB box was thought to exhibit a different conformation upon substrate binding (3). However, the conformation of the TonB box in the *in meso* structure, which was obtained without the substrate bound, is similar to that of the *in surfo* structure in the presence of substrate (3).

The conformation of the extracellular loops of OMP can be dramatically affected by the presence of ions in the extracellular medium (3,14). As the binding site for $B_{12}$ in BtuB is surrounded by extracellular loops, it is conceivable that a reversible change in the conformation of the extracel-lular loops in response to the extracellular makeup and ion concentration can serve as a mechanism for regulating substrate binding (15). Experimentally, the binding affinity of $B_{12}$ to BtuB in the outer membrane of E. *coli* was found to be 1000-fold higher at saturating levels of calcium than in its absence (16).

The 1NQG *in surfo* structure reveals three calcium ions in the extracellular loop region: two calcium ions bound to loops 3–4 and 5–6, and a third one bound to loop 15–16. Close inspection of the 1NQG crystallographic unit cell with Visual Molecular Dynamics (VMD) (17) revealed that the crystal contacts are not mediated by these calcium ions, and, hence, their presence may be of biological importance.

The role of the calcium ions located near loops 3–4 and 5–6 was thoroughly studied. Four aspartate residues forming the binding site for these ions are highly conserved among BtuB homologs (18). Point mutations in the binding site region were found to decrease substrate binding (16). Moreover, the B-factors of alpha carbon atoms, in the *in surfo* crystal structures with and without calcium ions, indicated that loops without bound calcium ions are more mobile and are more likely to occlude the pathway for substrate binding (3). In the *in meso* structure, loops 3–4 and 5–6 are not resolved, which may be associated with the absence of calcium in the *in meso* crystallization buffer. Thus, it is plausible that calcium ions near loops 3–4 and 5–6 stabilize the conformation of these loops (Fig. 1a) and thereby facilitate $B_{12}$ binding.

The role of the calcium ion located near loop 15–16 is unknown. In the *in meso* structure, loop 15–16 resides on the top of the barrel occluding the $B_{12}$ binding site. This conformation is in contrast with the conformation resolved in the *in surfo* model, where the loop is located at the edge of the barrel such that the $B_{12}$ binding site is exposed. Fig. 1b shows a top-view comparison of the conformations of loop 15–16 in the two X-ray structures. The different conformations of loop 15–16 may imply an additional mechanism for regulating $B_{12}$ binding by calcium.

In this manuscript we report MD simulations of three BtuB systems: the *in surfo* model with and without the calcium ions and the *in meso* model, all three embedded in a lipid bilayer membrane. Our ~100-ns simulations confirm the role of calcium ions in stabilizing the conformation of loops 3–4 and 5–6 and suggest an additional mechanism for regulating $B_{12}$ binding that involves loop 15–16. In all three systems, we observed partial unfolding of the TonB box, which suggests that their folded conformations resolved in the X-ray structures are likely caused by the crystallization conditions.

## Methods

### MD methods

All MD simulations were performed using the program NAMD (19), the CHARMM22 force field (20), periodic boundary conditions, particle-mesh Ewald (PME) full electrostatics and multiple time stepping (21) (1 fs for bonded interactions; 2 fs for unbonded short-range interactions; 4 fs for PME calculations of long-range couloumb interactions). The PME electrostatics were computed over a 100 × 100 × 120 grid (<1.3 Å grid spacing). The temperature was kept constant using a Langevin thermostat (22) coupled to all non-hydrogen atoms; the Langevin damping constant was set to 1 $PS^{-1}$. The integration time step chosen was 1 fs. The equilibration in the NPT ensemble was performed using Nosé-Hoover Langevin piston pressure control (23) at 1 bar. Van der Waals energies were calculated using a smooth (10–12 Å) cutoff. Restraints were imposed through harmonic forces using a spring constant of 1 kcal/($Å^2$ mol).

### Microscopic models of BtuB in a lipid bilayer membrane

We built atomic-scale models of BtuB in the *in surfo* and *in meso* conformations embedded in a lipid bilayer membrane. The atomic coordinates of the *in surfo* and *in meso* models were taken from their corresponding X-ray structures (PDB access codes 1NQG and 2GUF, respectively). The protein fragments missing in the above X-ray structures were modeled using coordinates of the most complete X-ray structure of BtuB, PDB access code 1NQH. The first five residues missing in the *in surfo* structure were modeled according to the *in meso* structure.

In addition to water resolved in the X-ray structures, additional water molecules were placed into internal cavities of the protein structures using the Dowser program (24). Following that, the Solvate program (25) was used to add a 3 Å layer of water around the protein. The protein

was merged with a patch of a pre-equilibrated and solvated palmitoyloleoylphosphatidylcholine (POPC) lipid bilayer containing 388 lipid molecules. All lipid molecules that overlapped with the protein were removed, as well as all water molecules around the protein that overlapped with the lipid bilayer.

The protein-lipid complex was solvated in a rectangular volume of pre-equilibrated TIPS3P (26) water molecules. $Na^+$ and $Cl^-$ ions were added at random positions, corresponding to a solution concentration of 0.12 M. The final systems measured about 125 × 125 × 130 $Å^3$, contained over 217,000 atoms, and were electrically neutral. Fig. 1 shows the final all-atom *in surfo* model of BtuB.

To remove possible steric clashes that might have been introduced during the assembly process, each system underwent 3,000 steps of minimization using a conjugate gradients method. Following that, the systems were equilibrated at 310 K in the NPT ensemble. In each system, the protein backbone was restrained during the first 0.5 ns of the equilibration. To ensure that the protein fragments that were modeled according to the 1NQH structure were properly aligned with the rest of the protein, each system was simulated for another 0.5 ns having all but the modeled part of the protein backbone restrained. The rest of the simulations were carried out in the NPT ensemble without applying any restraints.

To obtain a model of the *in surfo* structure without calcium ions, the four calcium atoms resolved in the original *in surfo* structures were removed, along with eight randomly chosen chloride ions, from a microscopic state obtained after ~ 18 ns of unrestrained equilibration of the original *in surfo* model. Starting from that state, the two *in surfo* models (with and without calcium ions) were simulated for approximately 70 ns in the NPT ensemble. To ensure proper equilibration of the system after removal of the calcium ions, the backbone of the protein was restrained for the first 0.5 ns. A summary of all simulations performed is shown in Table 1.

## Analysis of correlated motions

To investigate correlated motions in the BtuB structure, we computed the generalized correlation of the motion of BtuB in equilibrium. The generalized correlation, developed by Lange and Grübmuller (27), is based on the mutual information between the motion of atoms around their average position. The mutual information (27) tells us exactly how much information we can learn about the motion of one atom by measuring the motion of a second atom. Using this measure, we can learn more about the correlation between two atoms than in the standard covariant, or Pearson, measure. The generalized correlation detects correlated motion regardless of the relative orientation and includes nonlinear contributions, such as two atoms fluctuating sinusoidally but out of phase (27).

The generalized correlation analysis was performed over the last 50 ns of the equilibration trajectories of the *in surfo* (with and without calcium ions) and *in meso* systems. Each 50-ns trajectory was represented by 10,000 microscopic states. To remove all rotational and translational motion, the conformation of the protein in each frame of the trajectory was aligned to that of the *in surfo* X-ray structure using coordinates of its $\beta$-barrel as the reference. Because the generalized correlation measure is computationally intensive, we represented each residue by its $C_\alpha$-atom. We recorded the motion of each $C_\alpha$-atom around its average position and computed the generalized correlation between every atom pair using the g_correlation software developed by Lange and Grubmüller (27), with a density estimator nearest neighbor parameter $k = 6$ (28). To ensure that numerical instabilities did not result in spuriously low correlation values, we also computed the linear generalized correlation and used it as a minimal value for the generalized correlation measure, as recommended by Lange and Grübmuller (27).

## Results

### Conformational dynamics of the *in surfo* structure

Fig. 2*a* shows the average root mean square deviation (RMSD) of loop 15–16 from its X-ray coordinates during the simulations of the *in surfo* model performed with and without calcium ions. With the calcium ion bound on loop 15–16, the RMSD of that loop's backbone reaches 4.5 Å after ~ 15 ns and stays at this level until the end of this 90-ns simulation. The average RMSD of the flexible loops in other OMPs attain about the same value (13,15,29,30). As described in the Methods, calcium ions were removed from the state obtained after 18 ns of this simulation; a 72-ns simulation (with no calcium ions) was performed starting from this microscopic state. In the absence of calcium, the RMSD of loop 15–16 backbone from its X-ray coordinates saturates at 8.5 Å, which indicates that the original conformation of the loop is not stable in the absence of calcium.

Fig. 2b,c illustrates the conformations of the extracellular loops of the *in surfo* models simulated with and without the calcium ions. With a calcium ion bound, loop 15–16 fluctuates around the conformation resolved in the crystal structure, Fig. 2b. However, the same loop, loops 13–14 and 19–20 were observed to move toward the center of the $\beta$-barrel after the nearby calcium ion was removed, Fig. 2c. This motion substantially reduced the size of the entrance to the substrate binding site. Stabilized by two calcium ions, loops 3–4 and 5–6 were observed to reside at the edge of the barrel, although the tips of these loops were mobile. Once the two calcium ions were removed, loops 3–4 and 5–6 could still maintain their conformations because two sodium ions entered the calcium ion binding sites. Animations S1 and S2 in the Supporting Material illustrate the dynamics of the loops with and without calcium ions. However, in the simulation of the *in meso* structure (performed with no calcium ions, see below), the conformation of these loops was unstable and the loops could occlude the pathway to the substrate binding site.

Figure 3 shows the final conformations of the *in surfo* model in the simulations performed with and without calcium ions. In the presence of calcium, the entrance to the substrate binding site is wide open, Fig. 3*a*. However, upon removal of calcium ions, loop 15–16 tilts toward the barrel top and forms a contact with loop 19–20. This contact stabilizes the tilted conformation of loop 15–16 and causes partial occlusion of the $B_{12}$ binding site. Coincident with the above motion, other loops (for example, loop 13–14) moved toward the barrel's center. Figure 3c,d illustrates the electrostatic interactions between loops 15–16, 17–18 and 19–20 that might be responsible for the occlusion of the binding site. Loop 15–16 contains four negatively charged residues $Asp^{445}$, $Asp^{447}$, $Asp^{448}$ and $Glu^{456}$, while the neighboring loops, 17–18 and 19–20, contain three positively charged residues $Arg^{497}$, $Arg^{498}$ and $Lys^{529}$. Without a calcium ion bound to residues $Asp^{447}$ and $Asp^{448}$ in loop 15–16, $Lys^{529}$ and $Asp^{448}$ form a salt bridge, reducing the distance between loops 15–16 and 19–20. The tilted conformation of loop 15–16 (Fig. 3*d*) may facilitate the formation of the $Arg^{498}$–$Asp^{445}$ salt bridge, which is observed in the *in meso* structure. Limited by the time scale of our MD simulation, we observed only transient formation of this salt bridge. With a calcium ion bound to residues $Asp^{447}$ and $Asp^{448}$ at loop 15–16, the attraction between loops 15–16 and 19–20 is weakened and loop 15–16 can maintain its position at the barrel's edge, Fig. 3 *c*. Large fluctuations in RMSD of loop 15–16 with a bound calcium ion, Fig. 2 *a*, may be caused in part by the weak electrostatic forces between loops 15–16 and 19–20.

The results of our MD simulations are consistent with the experimental study of the loop's contributions to the substrate binding (31). In those experiments, deletion of residues $Ile^{444}$ through $Asp^{448}$ in loop 15–16 was observed to reduce the binding affinity of $B_{12}$ to BtuB by a factor of 50, presumably because of the removal of the calcium binding site. Residues

$Asp^{447}$ and $Asp^{448}$ that form a calcium binding site at loop 15–16 are highly conserved among BtuB homologs (18).

We have calculated generalized correlations between all the C$\alpha$ atoms in each simulated protein structure to further understand the observed loop dynamics in simulations. In Fig. 4 *a*, *b*, bright horizontal and vertical stripes (yellow or green) correspond mostly to the residues of the extracellular loops whose motion shows a high degree of correlation with the motion of other residues. Dark blue horizontal and vertical stripes correspond mainly to the periplasmic turns or the $\beta$-sheets in the barrel, which motion has low correlation with the motion of other residues. These maps indicate that the extracellular loops may play an important role in signal transduction after the substrate binding. The effect of having bound calcium ions can be studied using the difference of the correlation matrices (Fig. 4c). With bound calcium ions near loops 3–4 and 5–6, the motion of these two loops appear to be more correlated with the motion of residues in the hatch domain. Note that the $B_{12}$ binding site includes the top of the hatch domain and parts of loops 3–4 and 5–6. Therefore, calcium binding to loops 3–4 and 5–6 stabilizes the substrate binding site, which increases the binding affinity to the $B_{12}$. The enhanced correlation between these loops and the hatch domain also suggests stiffening of the protein structure, which is expected to promote signal transduction through the hatch domain. After the removal of the calcium ions, the motion in loop 15–16 becomes more correlated with the motion in other loops because loop 15–16 forms a contact with loop 19–20.

## Conformational dynamics of the *in meso* structure

In our MD simulations of the *in surfo* model, loops 3–4 and 5–6 were found to maintain their conformations when either calcium or sodium ions occupied the ion binding site harbored by those loops. The consequences of having that ion binding site empty was revealed in our simulation of the *in meso* model.

Figure 5 illustrates the conformations of the *in meso* model during a 60-ns MD simulation. No calcium ions were introduced into this simulation system. The calcium binding site in loops 3–4 and 5–6 was formed by four negatively charged residues: $Asp^{179}$, $Asp^{193}$, $Asp^{195}$, and $Asp^{230}$. Without cations at this binding site, the local electrostatic repulsion drove loops 3–4 and 5–6 apart within 30-ns of the MD simulation: loop 5–6 moved towards the barrel's center while loop 3–4 moved in the opposite direction. During this time, no sodium ions were observed to enter the calcium binding site, and hence the site's structure could deteriorate. Subsequently, loop 5–6 came in contact with loop 15–16, separating loop 15–16 from loop 19–20. Following that, loop 3–4 stretched out and came into contact with both loops 15–16 and 19–20. The contacts between these loops effectively covered the substrate binding site. This simulation, along with two simulations of the *in surfo* model, indicates that the two calcium ions residing in loops 3–4 and 5–6 stabilize these loops' conformation, which keeps the entrance to the substrate binding site open. It is worth noting that the initially disordered loop 7–8 folded into an alpha-helix during the course of the simulation, Fig. 5.

Without calcium ions, simulations of the *in meso* and the *in surfo* models show the similar trend to close the substrate binding pathway, as shown in the conformational changes of loops (Fig. 3 and Fig. 5). However, the final conformation of each loop in the *in meso* model is quite different from that in the *in surfo* model, indicating various ways for loops to occlude the $B_{12}$ binding site.

## Structural dynamics of the TonB box in the simulated models

A set of *in surfo* crystal structures of BtuB with and without the bound $B_{12}$ ligand captured different conformations of the TonB box (residues $Asp^{6}$-$Ala^{12}$), supporting the allosteric signaling hypothesis (3). However, the conformation of the TonB box resolved in the *in*

*meso* structure without the bound $B_{12}$ substrate is very similar to that observed in the *in surfo* structure with the substrate bound, which calls into question the proposed allosteric coupling between the binding of $B_{12}$ and the conformation of the TonB box. Here, we present analyses of the structural fluctuations of the TonB box observed in our three MD simulations.

Figure 6 shows conformational dynamics of the TonB box. The residues $Asp^6$, $Thr^7$ and $Leu^8$ show a stable backbone structure that has an "L" shape. In both *in surfo* models (with and without the calcium ions), these three residues are bent toward the hatch domain. In the course of our simulations, residue $Asp^6$ formed a salt bridge with residue $Arg^{106}$, which partially stabilized the conformation of residues $Asp^6$, $Thr^7$ and $Leu^8$. This salt bridge was observed to break and reform frequently. The conformation of residues $Asp^6$-$Leu^8$ in the *in meso* model was found to be stable in our MD simulation (Fig. 6). In this conformation, residues $Asp^6$-$Leu^8$ are bent towards the protein barrel, similar to the conformation resolved in the *in surfo* structure with the $B_{12}$ substrate bound (PDB code: 1NQH). The conformations of the TonB box in our simulations of the *in surfo* and the *in meso* models did not converge to the same structure, most likely, because of the insufficient time scale of our simulations (100 ns).

Structural stability of the TonB box and the adjacent residues is quantitatively characterized in Fig. 7. The RSMD of the TonB box's coordinates from the respective starting conformations, Fig. 7a, remains below 3 Å, indicating no dramatic changes in the conformation of the TonB box. Residues 1–5 in the *in surfo* model, which were not resolved in the X-ray structure and were modeled according to the *in meso* coordinates, show considerable flexibility, increasing the average RMSD of the last sixteen residues to about 5.5 Å. The RSMD of the same residues in the *in meso* model remains below 3 Å as the entire N-termial region preserves its conformation.

Fig. 7b shows per residue root-mean-square fluctuation (RMSF) of the TonB box about its average conformation over the last 50 ns of the respective simulations. The RMSF of the TonB box is small (<2 Å) in all three simulations. Such an ordered structure might be essential for the recognition of the TonB box by the protein TonB. The RMSF of residues 1–5 is high for the *in surfo* simulation performed in the absence of calcium ions. Surprisingly, the presence of calcium ions seems to dramatically stabilize the conformation of these residues, such that their RMSF are considerably lower than in the *in meso* structure. Both the RMSF and RMSD data indicate that the N-terminus of the *in surfo* model reached a new stable conformation in the simulation performed with all calcium ions bound. Visual inspection of the simulation trajectory with VMD revealed that this particular conformation of the N-terminus is stabilized by the salt bridge between $Asp^2$ and $Arg^{133}$, hydrogen bonds between $Gln^1$, $Asp^2$ and $Thr^3$ and $Glu^{135}$, and hydrogen bonds between $Gln^1$ and $Gln^{105}$, $Arg^{106}$ and $Thr^{30}$, the last group forming a pocket. Although it is tempting to speculate about the biological significance of this observation, a strong statement concerning the causal relationship between calcium binding and the stabilization of the N-terminus would be premature. Animations S3, S4 and S5 in the Supporting Material illustrate the dynamics of the TonB box and surrounding residues in the three simulations.

## Conclusion

Our simulations have elucidated the effect of calcium ions on the conformation of the extracellular loops in BtuB and their potential role in regulating substrate binding. Among the three calcium ions bound to the extracellular loops, the two ions bound to loops 3–4 and 5–6 are buried inside the molecular surface of the protein, while the calcium ion bound to loop 15–16 is exposed to the extracellular medium. Hence, it is likely that the occupancy of the binding site on loop 15–16 is more sensitive to the calcium level than that on loops 3–4 and 5–6. Furthermore, we have shown that loop 15–16 can adopt different conformations with and

without bound calcium ion, and that this change can affect the accessibility of the substrate binding site. A similar mechanism was suggested for the adhesin OMP OpcA: the structure of loops near the entrance to the ligand (sialic acid) binding site was found to depend on ion concentration (15). Thus, the proposed mechanism stipulates that binding of ions to the flexible loops of an OMP stabilizes the loops' conformations and leads to the formation of a relatively stable binding site or a pathway to the binding site that facilitates molecular recognition during substrate binding and increases binding affinity. More interestingly, in the case of BtuB, substrate docking can in turn affect calcium binding (14). The crystal structure of BtuB with a bound substrate (PDB code: 1NQH) revealed no calcium ion bound to loop 15–16. When the all-atom force field for $B_{12}$ becomes available, it will be of interest to investigate the interdependence of calcium and $B_{12}$ binding in BtuB.

## Acknowledgments

This work is supported by the grants from National Institutes of Health (PHS 5 P41 RR05969), National Science Foundation (PHY0822613), and the Petroleum Research Fund (48352-G6). The authors gladly acknowledge supercomputer time provided by the National Center for Supercomputing Applications via Large Resources Allocation grant No. MCA05S028. Grant support for MC was provided by the National Institutes of Health (GM75915) and Science Foundation Ireland (07/IN.1/B1836).

## References

1. Postle K, Kadner RJ. Touch and go: tying TonB to transport. Mol Microbiol 2003;49:869–882. [PubMed: 12890014]
2. Wiener MC. TonB-dependent outer membrane transport: going for Baroque? Curr Op Struct Biol 2005;15:394–400.
3. Chimento DP, Mohanty AK, Kadner RJ, Wiener MC. Substrate-induced transmembrane signaling in the cobalamin transporter BtuB. Nature Struct Biol 2003;10:394–401. [PubMed: 12652322]
4. Shultis DD, Purdy MD, Banchs CN, Wiener MC. Outer membrane active transport: structure of the BtuB:TonB complex. Science 2006;312:1396–1399. [PubMed: 16741124]
5. Cherezov V, Yamashita E, Liu W, Zhalnina M, Cramer WA, Caffrey M. mesoStructure of the Cobalamin Transporter, BtuB, at 1.95 Å Resolution. J Mol Biol 2006;364:716–734. [PubMed: 17028020]
6. Fanucci GE, Coggshall KA, Cadieux N, Kim M, Kadner RJ, Cafiso DS. Substrate-induced conformational changes of the perplasmic N-terminus of an outer-membrane transporter by site-directed spin labeling. Biochemistry 2003;42:1391–1400. [PubMed: 12578351]
7. Gumbart JC, Wiener MC, Tajkhorshid E. Mechanics of force propagation in TonB-dependent outer membrane transport. Biophys J 2007;93:496–504. [PubMed: 17449669]
8. Shultis DD, Purdy MD, Banchs CN, Wiener MC. Crystallization and preliminary X-ray crystallographic analysis of the Escherichia coli outer membrane cobalamin transporter BtuB in complex with the carboxy-terminal domain of TonB. Acta Cryst F 2006;62:638–641.
9. Caffrey M. Crystallizing Membrane Proteins for Structure Determination: Use of Lipidic Mesophases. Annu Rev Biophys 2009:38.
10. Caffrey M. Membrane protein crystallization. J Struct Biol 2003;142:108–132. [PubMed: 12718924]
11. Caffrey M, Cherezov V. Crystallizing membrane proteins using lipidic mesophases. Nat Protocols 2009;4:706–731.
12. Cherezov V, Liu W, Jeremy D, Luan B, Aksimentiev A, Katritch V, Caffrey M. In meso crystal structure and docking simulations suggest an alternative proteoglycan binding site in the OpcA outer membrane adhesin. Proteins: Struct, Func, Bioinf 2008;71:24–34.
13. Luan B, Caffrey M, Aksimentiev A. Structural refinement of the OpcA adhesin using molecular dynamics. Biophys J 2007;93:3058–3069. [PubMed: 17938421]
14. Bradbeer C, Gudmundsdottir A. Interdependence of Calcium and Cobalamin Binding by Wide-Type and Mutant BtuB Protein in the Outer Membrane of E*scherichia coli*. J Bacte-riol 1990;172:4919–4926.

15. Bond PJ, Derrick JP, Sansom MSP. Membrane simulations of OpcA: gating in the loops? Biophys J 2007;92:L23–L25. [PubMed: 17114231]
16. Cadieux N, Barekzi N, Bradbeer C. Observations on the Calcium Dependence and Reversibility of Cabalamin Transport across the Outer Membrane of E*scherichia coli*. J Biol Chem 2007;282:34921–34928. [PubMed: 17908684]
17. Humphrey W, Dalke A, Schulten K. VMD – Visual Molecular Dynamics. J Mol Graphics 1996;14:33–38.
18. Chimento DP, Kadner RJ, Wiener MC. The E*scherichia coli* outer membrane cobalamin transporter BtuB: Structural analysis of calcium and substrate binding, and identification of orthol-ogous transporters by sequence/structure conservation. J Mol Biol 2003;332:999–1014. [PubMed: 14499604]
19. Phillips JC, Braun R, Wang W, Gumbart J, Tajkhorshid E, Villa E, Chipot C, Skeel RD, Kale L, Schulten K. Scalable molecular dynamics with NAMD. J Comp Chem 2005;26:1781–1802. [PubMed: 16222654]
20. MacKerell AD Jr, Bashford D, Bellott M, Dunbrack RL Jr, Evanseck J, Field MJ, Fischer S, Gao J, Guo H, Ha S, Joseph D, Kuchnir L, Kuczera K, Lau FTK, Mattos C, Michnick S, Ngo T, Nguyen DT, Prodhom B, Reiher IWE, Roux B, Schlenkrich M, Smith J, Stote R, Straub J, Watanabe M, Wiorkiewicz-Kuczera J, Yin D, Karplus M. All-atom empirical potential for molecular modeling and dynamics studies of proteins. J Phys Chem B 1998;102:3586–3616.
21. Batcho PF, Case DA, Schlick T. Optimized particle-mesh Ewald/multiple-time step integration for molecular dynamics simulations. J Chem Phys 2001;115:4003–4018.
22. Brünger, AT. X-PLOR, Version 3.1: A System for X-ray Crystallography and NMR. The Howard Hughes Medical Institute and Department of Molecular Biophysics and Biochemistry, Yale University; 1992.
23. Martyna GJ, Tobias DJ, Klein ML. Constant pressure molecular dynamics algorithms. J Chem Phys 1994;101:4177–4189.
24. Zhang L, Hermans J. Hydrophilicity of cavities in proteins. Proteins: Struct, Func, Gen 1996;24:433–438.
25. Grubmüller H, Heymann B, Tavan P. Ligand binding and molecular mechanics calculation of the streptavidin-biotin rupture force. Science 1996;271:997–999. [PubMed: 8584939]
26. Jorgensen WL, Chandrasekhar J, Madura JD, Impey RW, Klein ML. Comparison of simple potential functions for simulating liquid water. J Chem Phys 1983;79:926–935.
27. Lange OF, Grubmüller H. Generalized correlation for biomolecular dynamics. Proteins: Struct, Func, Bioinf 2006;62:1053–1061.
28. Kraskov A, Stogbauer H, Grassberger P. Estimating mutual information. Phys Rev E 2004;69:066138.
29. Ash WL, Zlomislic MR, Oloo EO, Tieleman DP. Computer simulations of membrane proteins. Biochim Biophys Acta Biomembr 2004;1666:158–189.
30. Cox K, Bond PJ, Grottesi A, Baaden M, Sansom MSP. Outer membrane proteins: comparing X-ray and NMR structures by MD simulations in lipid bilayers. Eur Biophys J 2007;37:131–41. [PubMed: 17551722]
31. Fuller-Schaefer CA, Kadner RJ. Multiple Extracellular Loops Contribute to Substrate Binding and Transport by the E*scherichia coli* Cobalamin Transporter BtuB. J Bacteriol 2005;187:1732–1739. [PubMed: 15716445]

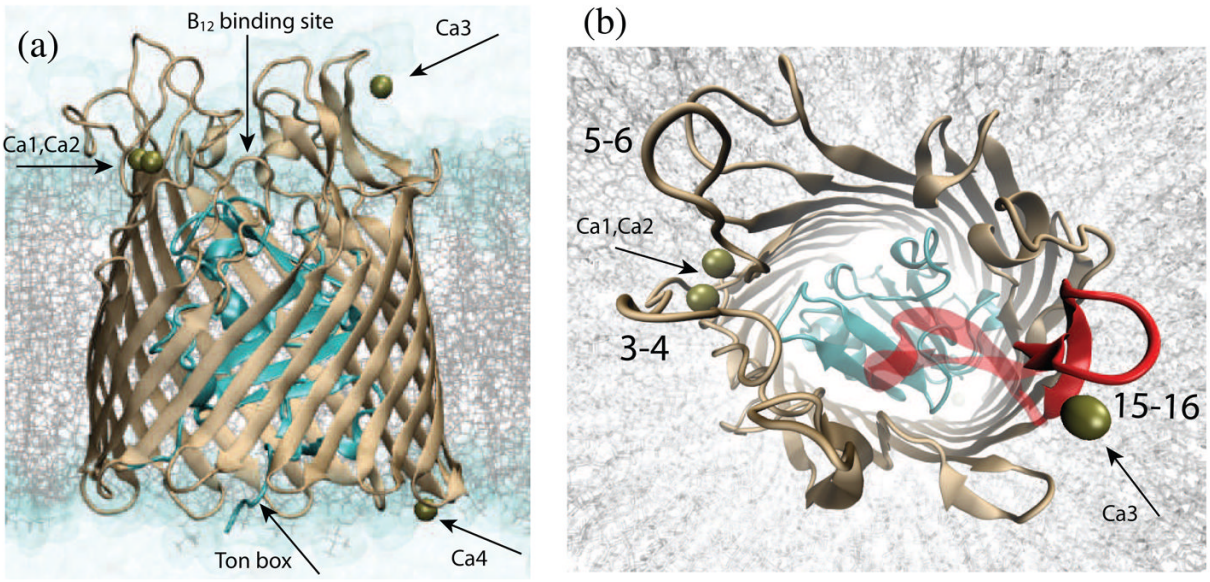


**Fig. 1.**

Microscopic model of BtuB in a lipid bilayer membrane. (a) Side view of the *in surfo* model (PDB ID: 1NQG). The barrel and the hatch domains are colored in brown and cyan, respectively. The lipid bilayer membrane (POPC) is drawn as grey lines; lipid molecules occluding the barrel were removed for clarity. Calcium ions resolved in the X-ray structure are shown as tan spheres. Water is shown as a transparent surface. (b) Top view of the *in surfo* model. Loop 15–16 of the *in surfo* model is highlighted in red; the same loop of the superimposed *in meso* model is shown as a transparent ribbon. In the *in meso* model, loop 15–16 covers the top of the barrel.

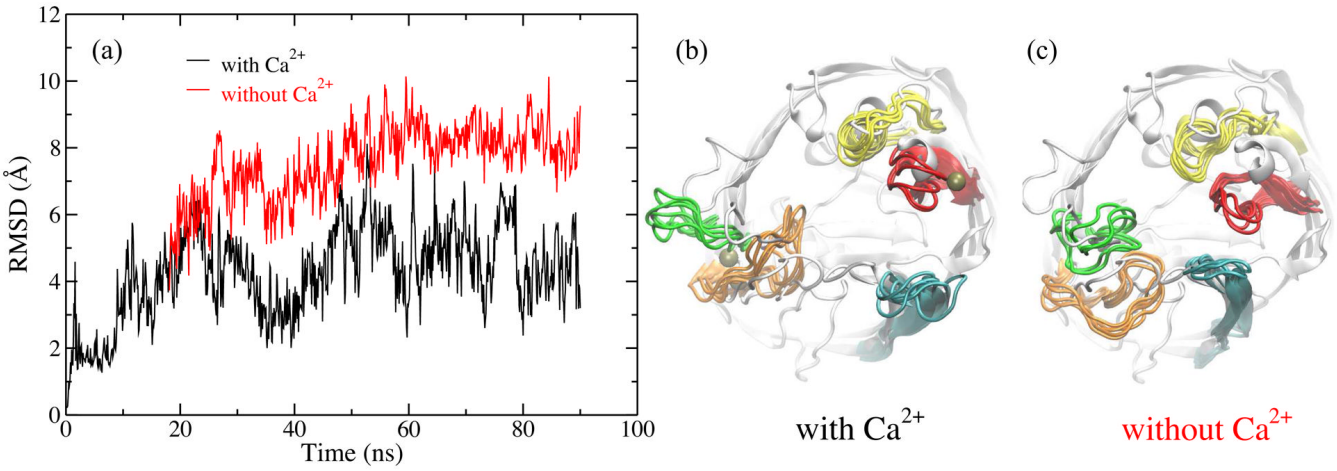


**Fig. 2.**

Effect of calcium on the conformation of the *in surfo* model. (a) Average RMSD of loop 15–16 with respect to the *in surfo* X-ray structure. The simulation with no calcium ions (red) started from the state obtained after 18 ns of the simulation performed with calcium ions (black). (b) and (c): The conformations of the extracellular loops within the last 20-ns of the simulations performed with and without calcium ions, respectively. The protein structure is shown in a cartoon representation. Loops 3–4, 5–6, 13–14, 15–16 and 19–20 that surround the B12 binding site are highlighted in orange, green, yellow, red and cyan; the rest of the protein is shown in white. For each 20-ns interval, five conformations (every 5 ns) of each loop are shown. In (b), calcium ions are shown as tan spheres.

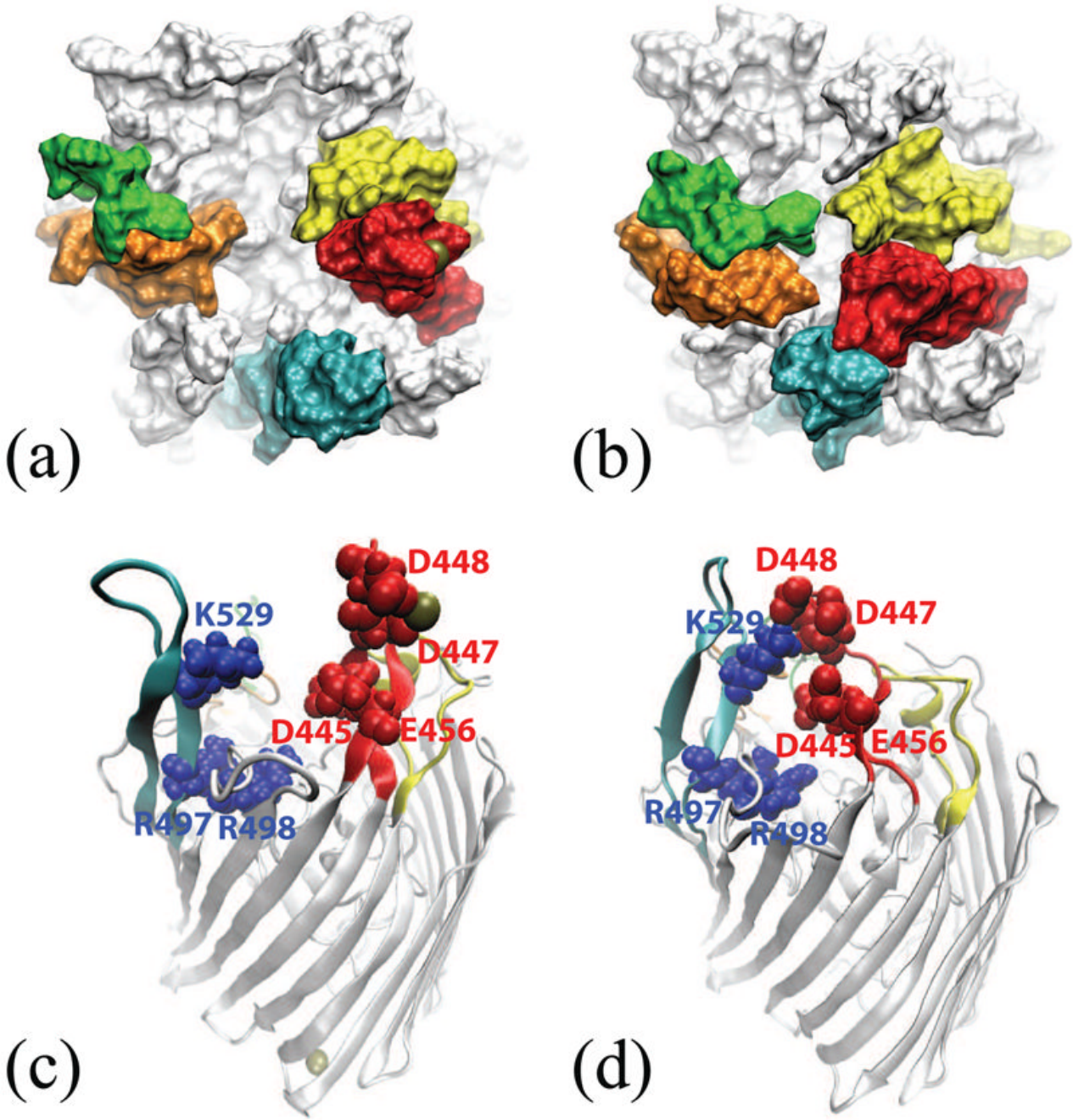


**Fig. 3.**

The effect of calcium on interaction between loops 15–16 and 19–20. Shown are equilibrated conformations of the *in surfo* model in the presence (a and c) and absence (b and d) of calcium ions. The loops are colored according to a scheme introduced in Fig. 2. A calcium ion is shown as a tan sphere. (a) and (b): The top views of the *in surfo* model. The protein structure is shown as a molecular surface. (c) and (d): Perspective view of the *in surfo* model. Charged residues of loops 15–16 and 19–20 are shown as blue (Arg and Lys) and red (Asp and Glu) van der Waals spheres. The rest of the protein is shown in a cartoon representation.

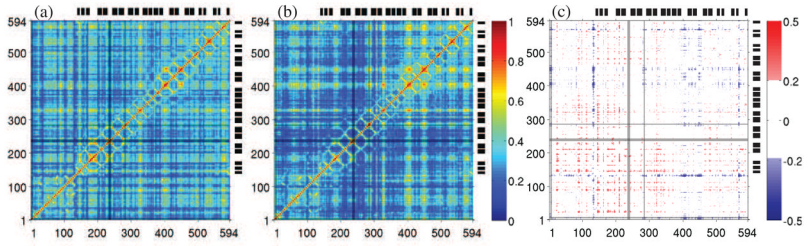


**Fig. 4.**

Correlation matrix for motion of $\alpha$-carbons in the *in surfo* model with (a) and without (b) bound calcium ions, respectively. The value of diagonal components (self-correlation) is 1.0. The matrix value is zero only if two residues are completely uncorrelated. (c) Differences in generalized correlations of $\alpha$-carbons between the *in surfo* models simulated with and without calcium ions. Red corresponds to a higher correlation in the system simulated with calcium, blue without. For the correlation difference map, only results for differences in correlation greater than atoms with distance less 0.2 are shown. Similarly, self-correlations and correlations between $C_\alpha$ than 7 Å have been removed. Correlations for residues which were missing in the crystal structure are highlighted in grey on the difference map. Black boxes alongside the correlation difference maps show the locations of the $\beta$-strands which compose the $\beta$-barrel.

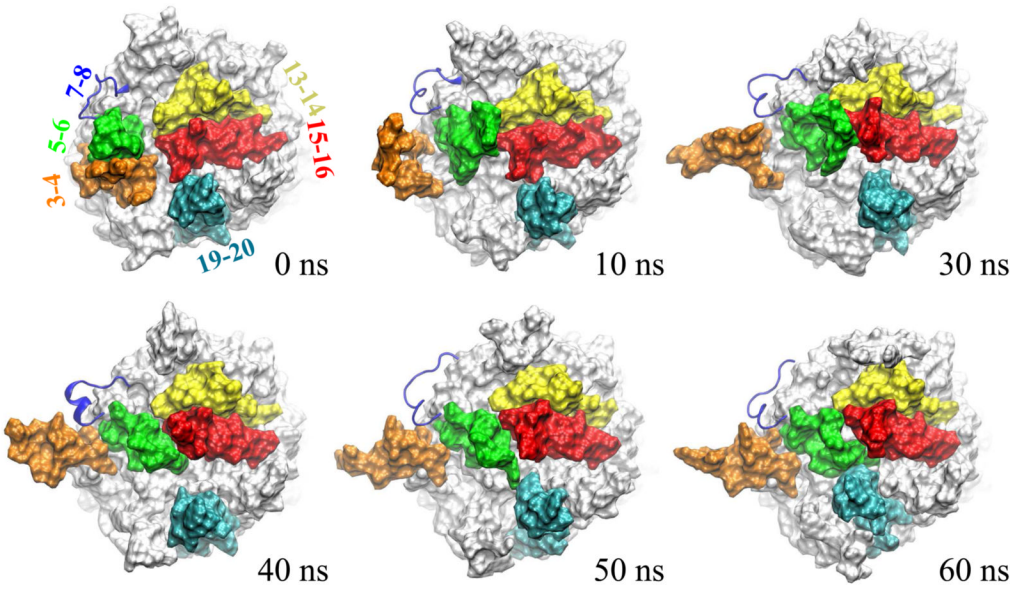


**Fig. 5.**

Loop conformations of the *in meso* model of BtuB during a 60-ns MD simulation. Loops 3–4, 5–6, 7–8, 13–14, 15–16 and 19–20 are colored in orange, green, blue, yellow, red and cyan. The protein is shown as a molecular surface, except for the loop 7–8, which is shown in a carto0n representation. During the simulation, loop 7–8 changed its secondary structure from a disordered cord to an alpha-helix. When neither calcium nor sodium ions occupied the ion binding site within loops 3–4 and 5–6, loop 5–6 moved toward the barrel's center and contacted loops 15–16 and 19–20. This motion occluded the $B_{12}$ binding site.

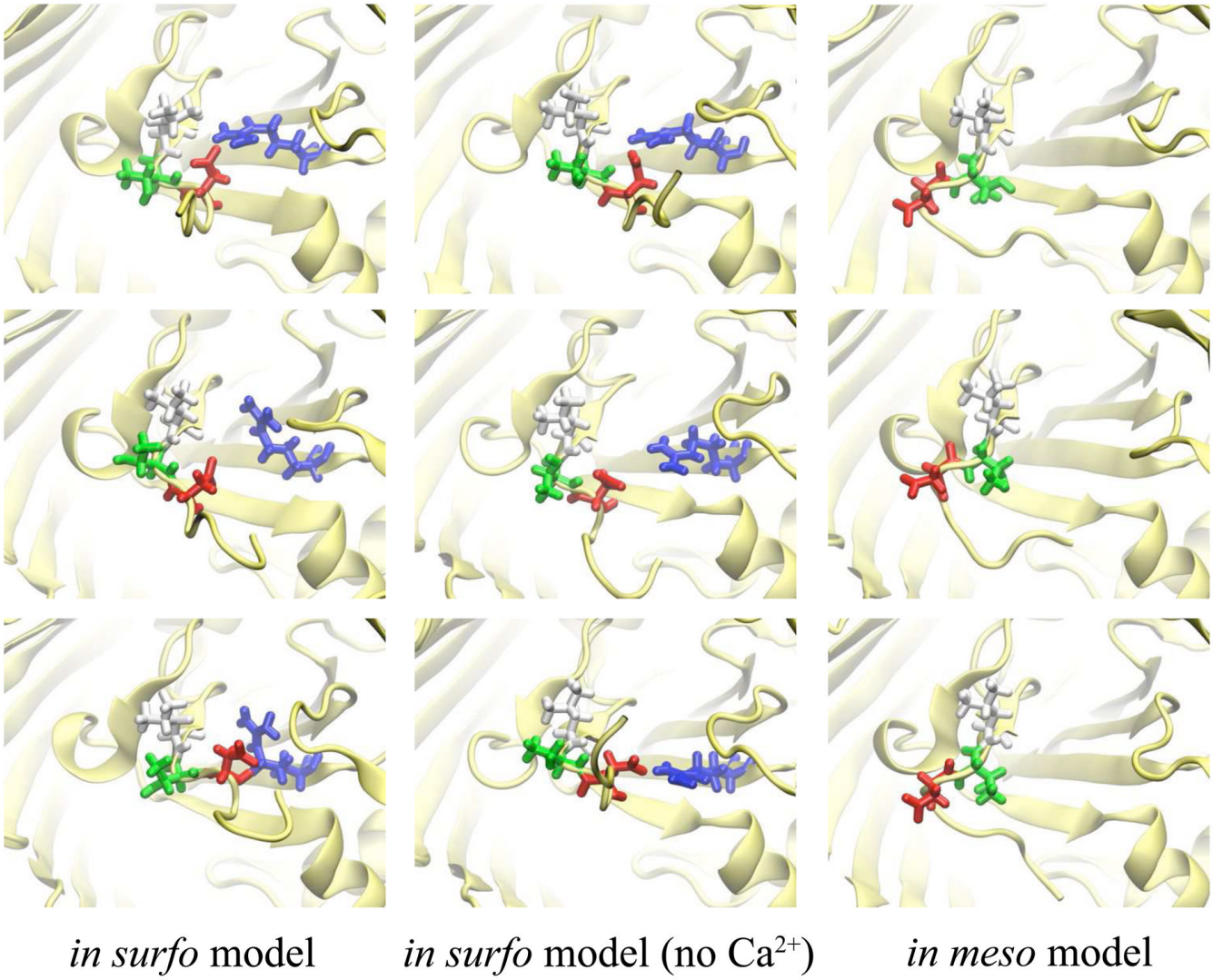


**Fig. 6.**

Conformational dynamics of the TonB box. The conformations of the TonB box in the MD simulations of the *in surfo* model with and without calcium are shown in the left and center columns, respectively. The right column corresponds to the simulation of the *in meso* structure. Representative conformations of the TonB box are shown at the beginning (top panels), in the middle (central panels) and at the end (bottom panels) of the respective simulation. Residues $Asp^{6}$ (red), $Thr^{7}$ (green) and $Leu^{8}$ (white) in the TonB box are highlighted in the stick representation. Residue $Arg^{106}$ (blue) was found to form a salt bridge with residue $Asp^{6}$, stabilizing the TonB box conformation in the *in surfo* model. Note that the TonB box of the *in meso* model is in a different conformation. Complete trajectories detailing the conformational dynamics of the TonB box are shown in Animations S3, S4 and S5.

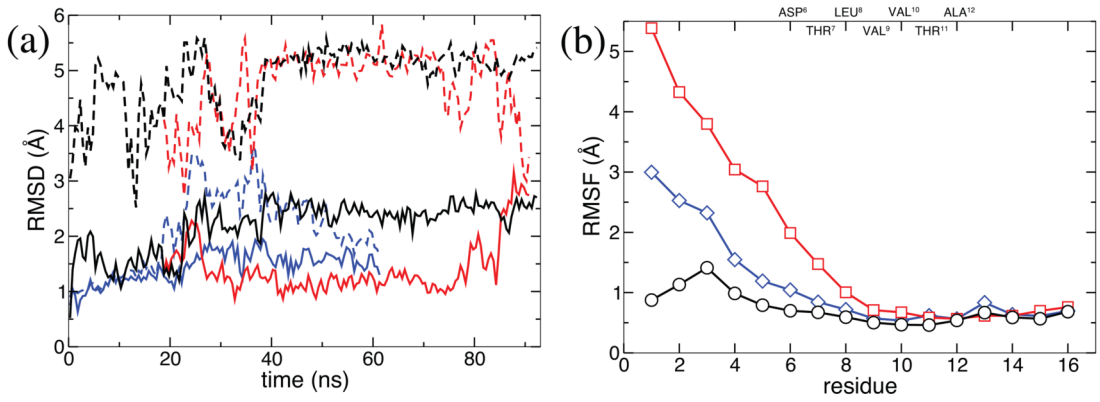


**Fig. 7.**

Dynamics of the TonB box. (a) Backbone RMSD of the TonB box (solid lines) and the first sixteen N-terminal residues (dashed lines) from the corresponding starting coordinates, including both crystal structure and modeled missing fragments, in the *in surfo* model simulated with (black) and without (red) calcium ions and in the *in meso* (blue) model. (b) RMSF of the first sixteen residues of the N-terminus about their average position during the last 50 ns of the simulations for the *in surfo* model with (black circles), and without (red squares) bound calcium ions and for the *in meso* (blue diamonds) model. The residue names of the TonB box are indicated along the upper axis.

## Table 1

Summary of all simulations performed.

| PDB Code | Crystallization Method | Presence of $Ca^{2+}$ | Time (ns) | # Atoms |
|---|---|---|---|---|
| 1NQG | *in surfo* | Yes | 92.6 | 217,550 |
| 1NQG | *in surfo* | No | 90.0 | 217,538 |
| 2GUF | *in meso* | No | 61.6 | 218,157 |